Theoretical Study of the Effect of Surface Density on the Dynamics of Ar + Alkanethiolate Self-Assembled Monolayer Collisions†

B. Scott Day, John R. Morris, William A. Alexander, and Diego Troya*

Department of Chemistry, Virginia Tech, 107 Davidson Hall, Blacksburg, Virginia 24061-0212

Received: July 21, 2005; In Final Form: October 3, 2005

We present a classical-trajectory study of energy transfer in collisions of Ar atoms with alkanethiolate self-assembled monolayers (SAMs) of different densities. The density of the SAMs is varied by changing the distance between the alkanethiolate chains in the organic monolayers. Our calculations indicate that SAMs with smaller packing densities absorb more energy from the impinging Ar atoms, in agreement with recent molecular-beam scattering experiments. We find that energy transfer is enhanced by a decrease in the SAM density because (1) less dense SAMs increase the probability of multiple encounters between Ar and the SAM, (2) the vibrational frequencies of large-amplitude motions of the SAM chains decrease for less dense SAMs, which makes energy transfer more efficient in single-encounter collisions, and (3) increases in the distance between chains promote surface penetration of the Ar atom. Analysis of angular distributions reveals that the polar-angle distributions do not have a cosine shape in trapping−desorption processes involving penetration of the Ar atom into the alkanethiolate self-assembled monolayers. Instead, there is a preference for Ar atoms that penetrate the surface to desorb along the chain-tilt direction.

Introduction

Understanding how a gas-phase species approaches, exchanges energy, and leaves a surface is the first step for a thorough characterization of gas/surface interfacial chemistry. Use of noble gases in elementary studies of gas/surface energy transfer is advantageous for many reasons, both experimentally and theoretically. At low collision energies, noble gases cannot produce chemical reactions that might obscure the determination of the energy-transfer step prior to or after reaction. In addition, the technology to produce molecular beams of noble-gas atoms with different collision energies in the laboratory is well-established,[1] which facilitates experimental measurements. Indeed, early experimental studies of collisions between noble gases and inorganic surfaces revealed the archetypal limiting pathways whereby gas-phase species interact with surfaces: the gas-phase species can recoil directly from the surface after a single encounter (impulsive scattering) or can interact with the surface during a prolonged period of time before returning to the gas phase (trapping−desorption).[2,3] From a theoretical perspective, the closed-shell nature of noble gases results in relatively simple noble-gas/surface potential energy surfaces characterized by a repulsive wall at short distances and a shallow van der Waals well at long distances. This simple profile of the potential energy surface can be modeled using straightforward pairwise Lennard-Jones or generalized exponential functions.[4] These simple potential-energy functions avoid the effort required to derive more complicated reactive multidimensional potential energy surfaces and allow one to integrate classical trajectories much faster than in direct-dynamics approaches.

Concerning the nature of the surfaces, the general ordered structure of most inorganic surfaces facilitates the connection between the scattering properties of the gas probe and the surface structure. In contrast, most organic surfaces are amorphous and their surfaces are rough, which significantly alters the gas/surface collision dynamics.[5−24] Alkanethiolate monolayers self-assembled on metal surfaces (SAMs) have an ordered, reproducible, and well-characterized structure,[25] representing an exception to the amorphous nature of most organic surfaces. These characteristics of alkanethiolate SAMs, in addition to their amenable synthetic routes,[26,27] have contributed to understanding energy transfer from gases to organic surfaces in recent time.[11−18]

One remarkable property of alkanethiolate SAMs is that their structure is preserved when the individual chains of the SAM are chemically modified to some extent.[28] This feature of SAMs has been recently exploited by Morris and co-workers to investigate how the chemical composition of the exposed region of the SAM affects gas/organic surface energy transfer.[13,15,16] Another attractive property of these organic surfaces is that *n*-alkanethiols adsorbed on gold and silver substrates present SAMs with identical chemical nature but different packing densities. Alkanethiolate SAMs on silver pack more tightly than on gold, with measurements indicating that whereas the separation between chains of SAMs on gold is 5.0 ± 0.2 Å,[29] chains of SAMs on silver are separated by 4.61 ± 0.15 Å.[30] The tighter packing of the SAMs leads to an increase in the interchain repulsive interactions, which results in a shift of the tilt angle from ∼30° for SAMs on gold[31] to ∼13° for SAMs on silver.[32] These SAMs were used by Day and Morris in a recent experimental study to investigate the extent of energy transfer from Ar atoms to organic films of identical chemical composition but different density.[33] The gas/surface molecular-beam scattering experiments revealed that argon atoms scattering from *n*-alkanethiolate monolayers adsorbed on silver substrates (high packing density) transfer less energy than from analogous monolayers formed on gold. The experiments were carried out for 80 kJ/mol Ar atoms impinging at 30° from the surface normal and scattering at the specular angle. Under these conditions, the fraction of Ar atoms that reach thermal equi-

† Part of the special issue "William Hase Festschrift".

* To whom correspondence should be addressed. E-mail: troya@vt.edu.

10.1021/jp054043j CCC: $33.50
Published on Web 11/05/2005

TABLE 1: Geometric Characteristics of the SAMs Used in This Work

interchain separation/Å	surface area per molecule/Å^2	tilt angle[a]/deg	height[a,b]/Å
4.30	16.0	4	15.3
4.67	18.9	17	14.5
4.98	21.5	30	13.2
5.20	23.6	35	12.2
5.40	25.3	36	11.8

[a] Average values during a 0.5 ns canonical simulation at 300 K. [b] Distance in the surface normal axis between the sulfur atom and the C atom of the methyl terminus.

librium with the surface is ≈15% smaller if the SAMs are grown on silver. In addition, the average energy transferred in impulsive collisions is lower by about 7% for the SAMs on silver.

In this paper, we present the results of classical-trajectory calculations aimed at providing atomic level details and augmenting the experimental information on energy transfer from Ar to SAMs of different densities. We calculate collisions of Ar with alkanethiolate SAMs constructed with the same lattice spacing as experimental SAMs on gold and silver, and with larger and smaller lattice spacings, in an attempt to rationalize and generalize the trends observed in the experiments.

Computational Details

We have integrated classical trajectories using an accurate potential energy surface derived by us in an earlier study of energy transfer in Ar + SAM collisions.[34] This potential energy surface was constructed by separately considering the interactions between the Ar atom and the SAM (intermolecular potential) and the interactions within the SAM (intramolecular potential). To incorporate accurate all-atom potentials in the region of the SAM that interacts directly with the striking Ar atoms, we divided the SAM into two regions, the ethyl termini and the rest of the SAM. The intramolecular potential for the ethyl termini of the SAM chains is described using the all-atom version of the OPLS force field (OPLSAA),[35] whereas the more interior region of the SAM is described using the united-atom version of the OPLS force field (OPLSUA).[36,37] This hybrid all-atom/united-atom model of the SAM allows us to describe the intermolecular interactions between the SAM terminus and the Ar atom using a very accurate all-atom potential derived from high-quality ab initio calculations[4] without dramatically increasing the computational overhead. The interactions between the Ar atom and the methylene units of the SAM below the two outermost C atoms are treated using the nonbonding terms of the OPLSUA force field. Earlier calculations of scattering-angle-dependent energy transfer in collisions of Ar with SAMs at 56 kJ/mol demonstrated that this hybrid surface had superior accuracy to surfaces used in prior studies,[18] which used an intermolecular potential energy surface derived from gas-phase experiments.[38] Further details of this model potential energy surface can be found in ref 34.

To study the effect of the SAM density on the dynamics of energy transfer, we have scattered Ar from five dodecanethiolate SAMs of different densities. The separations between the hydrocarbon chains in the five SAMs are 4.30, 4.67, 4.98, 5.20, and 5.40 Å. The SAMs with interchain separations of 4.67 and 4.98 Å mimic experimental SAMs grown on silver and gold, respectively. Although the rest of the SAMs constructed here cannot be directly connected with experimental SAMs, the rapid growth in self-assembled-monolayer technology might make it possible to build SAMs with custom interchain separations soon. Table 1 shows the characteristics of the five SAMs considered in this work. The data in the table indicate that larger interchain separations (lower densities) lead to larger tilt angles. Our calculations of the tilt angles for the SAMs with 4.67 and 4.98 Å lattice spacings are in agreement with the experimentally determined tilt angles for SAMs on silver and gold, respectively.[29,31] This agreement in the tilt angle gives us confidence about the accuracy of the intramolecular term of our potential energy surface for SAM packings other than those corresponding to SAMs on gold and silver surfaces.

It should be noted that the metal surfaces are not explicitly considered in this work. Instead, the sulfur atoms are held fixed to their minimum-energy locations for each SAM while the trajectories are evolving. The good agreement between theory and experiment noted in earlier work using this model demonstrates that neglecting the metal surface is a good approximation in studies of noble-gas scattering from dodecanethiolate SAMs.[34] Further support for this approximation is given by the recent experiments of Day and Morris,[14] which showed that the dynamics of energy transfer in Ar + SAM collisions is essentially independent of the alkanethiolate length for chains containing more than seven methylene units.

We have calculated batches of 1000 trajectories for each of the five dodecanethiolate SAMs described in Table 1 at collision energies (E_{coll}) of 60 and 80 kJ/mol and polar incident angles (θ_i) of 30 and 60° with respect to the surface normal. The trajectories are started at ≈20 Å from the impact point, which guarantees at least a 10 Å initial separation between the Ar atom and the closest atom of the SAM even at the most glancing incident polar angle ($\theta_i = 60°$). The initial conditions (coordinates and momenta) of the surface are taken from a 0.5 ns canonical simulation of the SAM at 300 K. The impact points on the surface are randomly selected from a region of the SAM twice the size of the unit cell defined by the rhombus formed by four adjacent sulfur atoms. In the scattering calculations, we use SAMs composed of 36 dodecanethiolate molecules that are replicated in two dimensions using the periodic-boundary-conditions algorithm of the TINKER package of programs.[39] The initial azimuthal angle formed by the velocity vector of the impinging Ar atom and the direction of the dodecanethiolate chains is randomly sampled to establish fair comparisons with experiments. In the experiments of Day and Morris,[33] the SAMs are grown on polycrystalline gold surfaces and involve different domains rotated with respect to one another, which in turn corresponds to a random sampling of the initial azimuthal angle since the size of the experimental argon beam is ≈1 cm^2.

The trajectories are stopped when the smallest internuclear distance between the Ar atom recoiling from the SAM and any atom of the SAM is larger than ≈10 Å. In some trajectories, the Ar atom becomes trapped on the surface for longer times than we can integrate. To avoid integrating these exceedingly long trajectories, we introduce a 15 ps cutoff in the trajectories propagation. If Ar does not desorb into the gas phase before that time, we assume that the Ar desorption is thermal. The Ar translational energy is then sampled from a Maxwell−Boltzmann distribution at the surface temperature (300 K), the polar scattering angle from a cosine distribution, and the final azimuthal angle (angle formed between the projections of the initial and final Ar velocity vectors on the surface plane) from a uniform distribution from 0 to 360°. The percentage of trajectories that do not desorb after 15 ps are as follow: 0.4, 5.1, 9.6, 17.3, and 25.9% for Ar collisions with a 30° incident angle on SAMs with 4.3, 4.67, 4.98, 5.2, and 5.4 Å lattice spacings, respectively, and 0.9, 2.0, 5.6, 8.4, and 15.3% for Ar collisions with a 60° incident angle on the same SAMs.

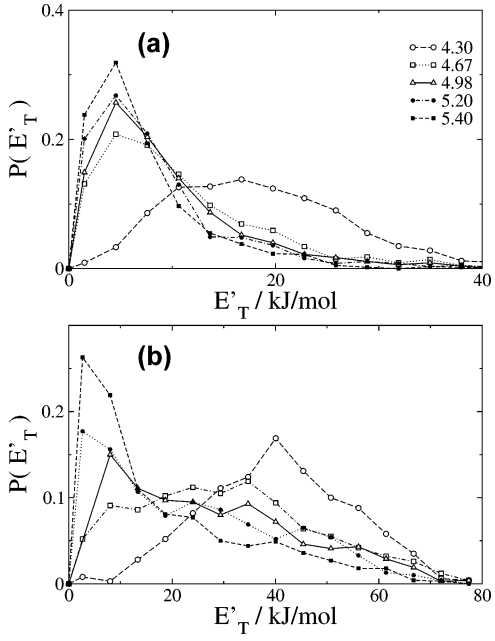

Figure 1. Product translational energy distributions in collisions of Ar with dodecanethiolate SAMs of different lattice spacings at E_{coll} = 80 kJ/mol. Incident angle: (a) 30 and (b) 60°. The legend indicates the lattice spacings in angstroms.

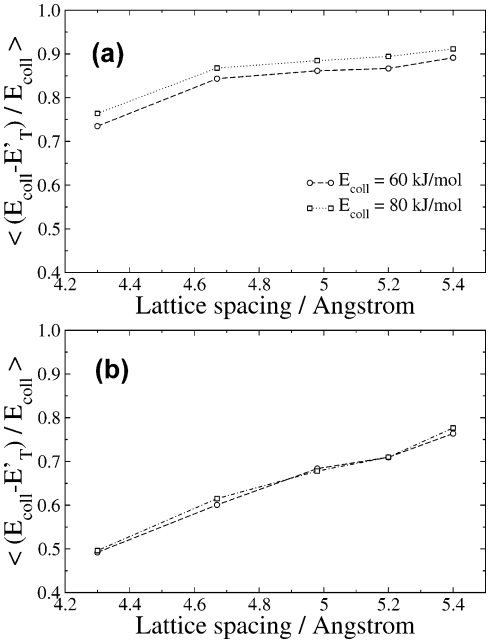

Figure 2. Average fractions of energy transfer in collisions of Ar with dodecanethiolate SAMs at E_{coll} = 60 and 80 kJ/mol as a function of the lattice spacing of the SAMs. Incident angle: (a) 30 and (b) 60°.

Results and Discussion

(a) Product Translational Energy Distributions. Figure 1 shows the product translational energy (E'_T) distributions (PTDs) of Ar scattering from SAMs with different lattice spacings calculated at E_{coll} = 80 kJ/mol with incident polar angles of θ_i = 30 and 60° (Figure 1a,b, respectively). The figure shows a clear correlation between the SAM density and the amount of energy transferred by the striking Ar atom. The calculations show that less dense SAMs promote energy transfer, which concurs with experiments.[33] At θ_i = 30°, there is a sharp difference between the PTD of the SAM with a 4.3 Å lattice spacing and the rest of the SAMs. The PTD of this highest-density SAM is much broader and peaks at an energy ≈15 kJ/mol larger than the rest of the SAMs. In the less dense SAMs, there is a smooth increase in the population of the low-energy region of the distributions with increasing lattice spacing. The same trend is observed with θ_i = 60° (Figure 1b), but the transition in the profile of the PTD from short to long lattice spacings is more gradual than with θ_i = 30°.

The traditional way to analyze the PTDs measured in scattering of Ar from SAMs on gold is to ascribe the low-energy region of the PTDs to thermalization of Ar on the surface and to relate the high-energy tail of the distribution to impulsive-scattering events.[33] If that picture captures the scattering dynamics of Ar from the SAMs studied in this work, we can see that decreasing the lattice spacing removes the thermal channel. In effect, for a lattice spacing of 4.3 Å and E_{coll} = 80 kJ/mol, the PTDs peak at an energy much larger than the thermal energy at the surface temperature ($kT \approx 2.5$ kJ/mol) both at θ_i = 30 and 60°. On the other hand, increases in the lattice spacing lead to an abrupt decrease in the population of the high-energy tail (particularly for θ_i = 30°) that makes the PTDs resemble Maxwell−Boltzmann distributions.

Figure 1 also displays the expected trend that more glancing collisions (collisions with larger incident angle) inhibit energy transfer. For instance, for a 4.3 Å lattice spacing, the peak of the PTD occurs at ≈17 kJ/mol for θ_i = 30° and at 40 kJ/mol at θ_i = 60°. For a 4.67 Å lattice spacing, whereas the PTD is dominated by the thermal component for θ_i = 30°, the PTD peaks at superthermal energies (≈30 kJ/mol) for θ_i = 60°. For the SAMs with the longest lattice spacings, the peak of the distributions occurs at thermal energies for both θ_i = 30 and 60°, but the PTDs with θ_i = 60° are much broader and have substantial population at very high product energies.

Figure 2 shows average fractions of energy transfer as a function of lattice spacing at E_{coll} = 60 and 80 kJ/mol for θ_i = 30° (Figure 2a) and θ_i = 60° (Figure 2b). As it can be inferred from the PTDs of Figure 1, the average fraction of energy transfer increases with increasing lattice spacing for both incident angles. The increase in the average fraction of energy transfer with lattice spacing is quasilinear for θ_i = 60°. For θ_i = 30°, there is a clear difference between the average fraction of energy transfer at a 4.3 Å lattice spacing and the values at the rest of the lattice spacings. It should be noted that if all the incident argon atoms were to reach thermal equilibrium with the surface before desorbing back into the gas phase, their average final energy would be ≈5 kJ/mol, on the basis of a 300 K flux-weighted Maxwell−Boltzmann distribution. This translates into energy-transfer fractions of 0.92 and 0.94 for E_{coll} = 60 and 80 kJ/mol, respectively. Figure 2a shows that, for a lattice spacing of 5.4 Å, the calculated values are very close to the limiting values. This finding implies that nearly all of the Ar atoms that strike a SAM with a 5.4 Å lattice spacing at a 30° incident angle thermalize on the surface, irrespective of their initial collision energy. On the other hand, a large fraction of the Ar atoms striking the various SAMs with θ_i = 60° do not fully thermalize even with the lowest-density SAMs. In the following section, we rationalize these trends in the energy-transfer efficiency by investigating the microscopic mechanism of the gas/surface collisions.

(b) Microscopic Mechanisms of Ar + SAM Collisions. To connect the extent of energy transfer with the microscopic details of the collisions, we distinguish among three types of events: (1) impulsive scattering, (2) trapping-desorption, and (3) direct penetration of the surface. The three mechanisms can be separated by the behavior and the value of the coordinate of the Ar atom in the axis defined by the surface normal

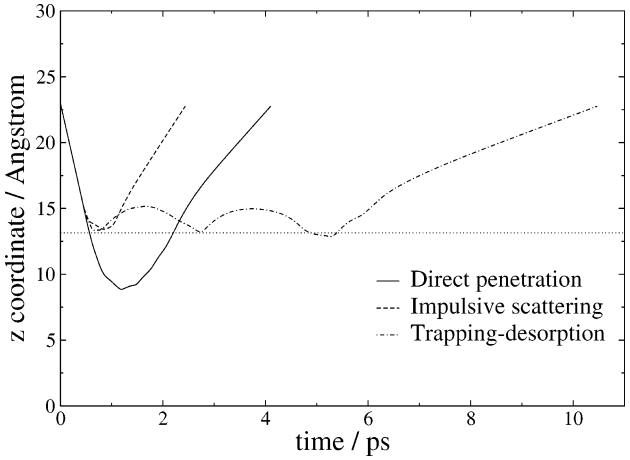

Figure 3. Illustrative representations of the variation with time of the value of the Ar atom coordinate in the axis defined by the surface normal (*z*-coordinate) for impulsive scattering, trapping−desorption, and direct penetration mechanisms. The initial conditions of the trajectories are $E_{coll} = 80$ kJ/mol, lattice spacing = 5.40 Å, and incident angle = 30°. The horizontal dotted line represents the average location of the terminal C atoms of the SAM.

(*z*-coordinate hereafter). In impulsive-scattering events, there is only one inner turning point in the Ar *z*-coordinate, and its minimum value is never below 1 Å of the average *z*-coordinate of the SAM $-CH_3$ terminal groups (i.e., Ar bounces only once on the surface and does not penetrate). In trapping−desorption processes, there are several inner turning points of the Ar *z*-coordinate. This behavior corresponds to collisions in which the Ar atoms ricochet across the surface for some time before desorbing back into the gas phase. The Ar atoms might or might not penetrate the SAM while they are trapped on the surface. In direct penetration, there is only one inner turning point in the *z*-coordinate of the Ar atom. However, the Ar atom reaches regions of the SAM 1 Å below the average *z*-coordinate of the $-CH_3$ terminal groups of the SAM (i.e., Ar penetrates the surface but bounces only once). Figure 3 shows illustrative representations of the three types of microscopic mechanisms considered here for collisions of Ar with SAMs.

The probability distributions of the number of inner turning points at $E_{coll} = 80$ kJ/mol for the five SAMs considered in this work are displayed in Figure 4 for $\theta_i = 30$ and 60°. The distributions show that increasing the lattice spacing between the alkanethiolate chains of the SAM increases the probability for a larger number of turning points. For $\theta_i = 30°$, almost all of the collisions bounce only once on the 4.3 Å SAM, whereas more than half of the collisions bounce at least twice on the 5.4 Å SAM. For $\theta_i = 60°$, the increase in the probability for multiple collisions with increasing lattice spacing is not as sharp as for $\theta_i = 30°$, but the trend can nonetheless be clearly observed. We showed in a previous study that, on the average, more energy is transferred in trajectories in which the Ar atom bounces many times on the SAM (several inner turning points) than in trajectories in which Ar recoils from the surface immediately after the initial impact (one inner turning point). (See Figure 4 of ref. 34.) Thus, the increase in average energy transfer with increasing lattice spacing seen in Figures 1 and 2 can be partially understood by an increase in the number of turning points (and therefore residence time) of the Ar atom on the surface of SAMs with longer lattice spacings.

The origin of the increase in the number of turning points with decreasing SAM density is manifold. Increasing the distance between chains makes the SAM surface more corrugated, which facilitates multiple encounters between the noble-gas atom and the hydrocarbon surface.[6] In addition, we show below that, even for collisions with a single turning point, energy transfer is more efficient if the distance between the chains in the SAM is increased. In single collisions with tightly packed SAMs, the Ar atoms will retain a significant part of their initial energy and escape the attractive potential of the SAM. On the other hand, in a loosely packed SAM, the Ar atoms will not retain as much of their collision energy and, in some cases, will not be able to overcome the attractive potential of the SAM instantaneously. Instead, the Ar atoms will become trapped on the surface before desorbing. Finally, an increase in the lattice spacing enhances the attractive interactions between Ar and the SAM at short distances above the surface.

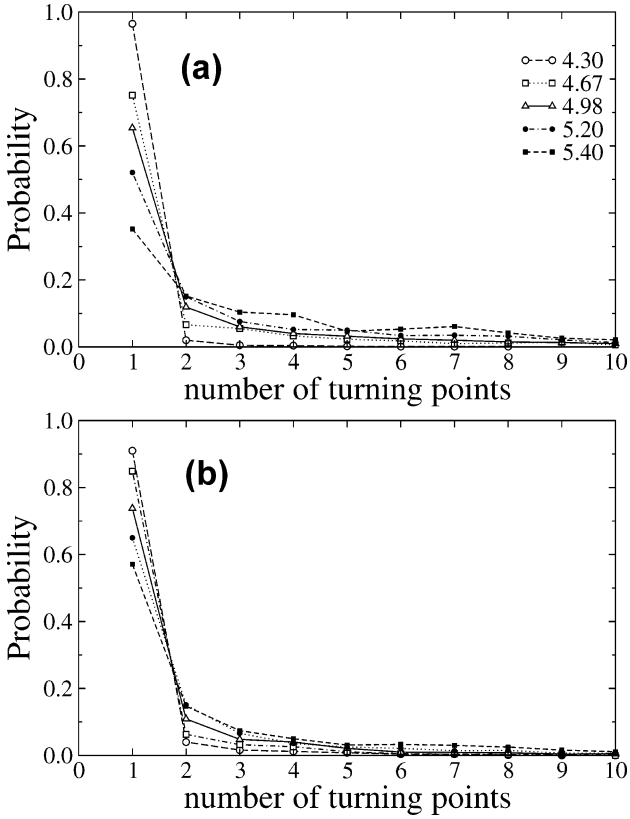

Figure 4. Probability distributions of the number of inner turning points of the Ar atom coordinate in the surface normal axis in collisions of Ar with dodecanethiolate SAMs at $E_{coll} = 80$ kJ/mol for different lattice spacings of the SAMs. Incident angle: (a) 30 and (b) 60°. The legend indicates the lattice spacings in angstroms.

To illustrate the latter point, we have scanned the intermolecular potential energy surface for various approaches of Ar to the SAMs. The absolute minimum-energy approach is that in which Ar is centered on the hollow site of the triangle formed by three adjacent chains of the SAM. Figure 5 shows the potential energy along that approach for SAMs with 4.98, 5.2, and 5.4 Å lattice spacings at different heights from the plane defined by the terminal C atoms of three adjacent chains. Clearly, the less dense SAMs exhibit deeper wells, and the wells are located at shorter distances between the Ar atom and the SAM. In addition, the figure also shows that the wells are wider with increasing lattice distance. This means that Ar feels an attractive potential from a larger region of the surface with less dense SAMs. The more attractive character of the less dense SAMs makes it more difficult for Ar atoms to escape the surface, contributing to the enhanced number of turning points (and therefore energy transfer) seen in Figure 4.

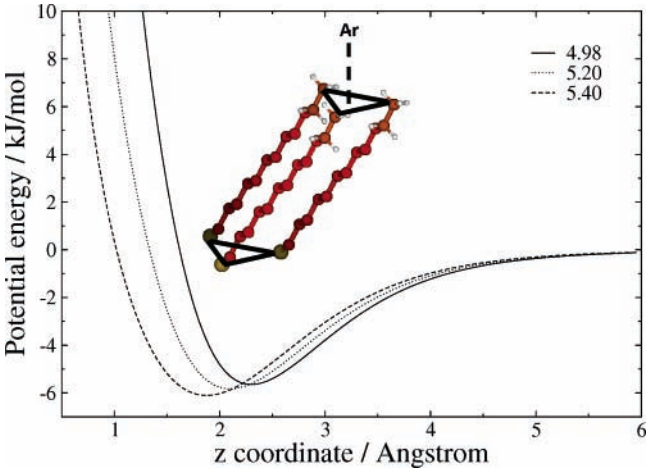

Figure 5. Intermolecular Ar + SAM potential energy for approaches of Ar to the hollow site formed by three adjacent chains in an alkanethiolate SAM for SAMs with different lattice spacings. The Ar atom approaches perpendicularly to the plane formed by the three terminal C atoms. The tilt angle of the chains is held fixed at 35° in the energy calculations of the three SAMs.

To delve further into the origin of the increased energy transfer to the SAM with increasing lattice spacing, we plot in Figure 6 the average fraction of energy transfer for trajectories that have only one turning point. These trajectories correspond to both the impulsive scattering and direct penetration mechanisms described above. The figure shows that the energy transferred from Ar to the SAM in trajectories with only one inner turning point depends on lattice spacing. This is particularly true for collisions at $E_{coll} = 60$ and 80 kJ/mol with a 60° incident angle, where the average fractions of energy transfer increase monotonically with lattice spacing. A similar trend is observed for a 30° incident angle when going from 4.3 to 4.67 Å lattice spacings. At that incident angle and for lattice spacings larger than 4.67 Å, the average fractions of energy transfer do not change appreciably with increasing lattice spacing for both 60 and 80 kJ/mol collision energies.

A possible reason for the increased energy transfer with lattice spacing in single collisions is rooted in the nature of the surface modes initially receiving the energy from the gas-phase species. Hase and co-workers showed that efficient energy transfer takes place when the excitation is channeled into low-frequency, large-amplitude modes of the surface (wags, torsions).[20,24] Increasing the distance between chains in the SAM leads to a decrease in the frequency of these large-amplitude vibrations. In effect, in more loosely packed SAMs, the nonbonding repulsions between chains decrease. As a result, the potential energy does not increase as sharply with interchain motions, which in turn decreases the vibrational frequency of the associated modes. To quantify the decrease in the vibrational frequencies of large-amplitude modes with increasing lattice spacing, we have calculated the harmonic vibrational frequencies of one dodecanethiolate chain in SAMs with 4.98, 5.2, and 5.4 Å lattice spacings. The calculations have been performed using the universal force field[40] as implemented in the Gaussian03 suite of programs.[41] For the sake of consistency, the calculations have been carried out by fixing the tilt angle of the chains to 35° for all of the SAMs. Three of the examined modes are presented here as exemplars of the decrease in the frequency of the large-amplitude motions that become excited upon collisions with Ar atoms. The frequencies of the wagging normal mode in the plane of the chain are 76, 99, and 121 cm^{-1} for SAMs with 5.4, 5.2, and 4.98 Å lattice spacings. The out-of-plane wagging motion

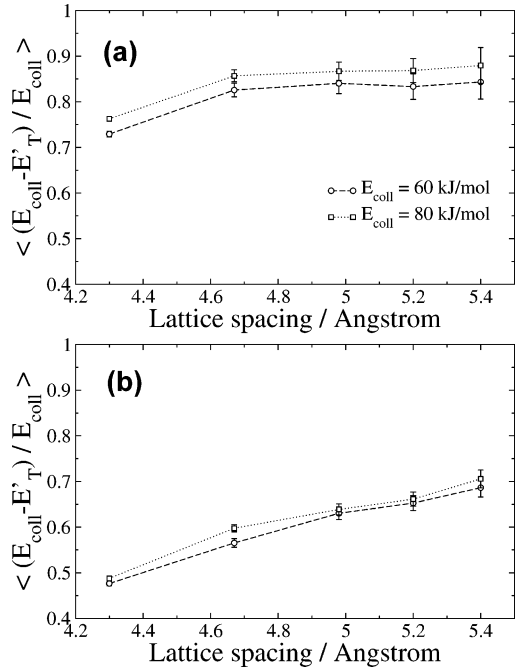

Figure 6. Average fractions of energy transfer in collisions of Ar with dodecanethiolate SAMs with one inner turning point at $E_{coll} = 60$ and 80 kJ/mol as a function of the lattice spacing of the SAMs. Incident angle: (a) 30 and (b) 60°.

frequencies are 39, 44, and 60 cm^{-1} for the same SAMs. Finally, the frequencies of a C−C−C bending motion that involves the upper half of the chains are 197, 228, and 324 cm^{-1} for the 5.4, 5.2, and 4.98 Å lattice spacings. It is well-known that decreases in the vibrational frequencies of molecular modes coupled to the reagent's translational coordinate lead to enhanced energy transfer.[42,43] Therefore, we conclude that the lowering in the frequencies of large-amplitude motions of the SAM with increasing lattice spacing contributes to the trend that less dense SAMs absorb more energy in single-encounter collisions, as observed in Figure 6. We note that using a harmonic normal-mode analysis of a single chain is only an approximation to model what happens in the majority of the single-collision trajectories. Customarily, Ar interacts directly with up to four SAM chains in single-encounter trajectories, all of which can absorb energy. In addition, a harmonic approximation is only valid if the energy transfer occurs in a time scale much shorter than that for intramolecular vibrational-energy redistribution (IVR).[24] So, the harmonic analysis can only be used to shed light in the steps of energy transfer prior to IVR.

We now turn our attention to the dynamics of Ar + SAM collisions in which Ar undergoes direct penetration of the surface. Our calculations reveal the expected trend that Ar can more easily penetrate the SAM below the methyl termini and rebound directly into the gas phase in collisions with SAMs of increasing interchain separation. With $\theta_i = 30°$ we do not see trajectories penetrating SAMs with 4.3 and 4.67 Å lattice spacings at either $E_{coll} = 60$ or 80 kJ/mol. At 5.2 and 5.4 Å lattice spacings, we find that ≈2 and 5% of the trajectories directly penetrate the surface and promptly desorb into the gas phase, irrespective of the initial collision energy. Direct penetration is strongly dependent on the incident angle, and with $\theta_i = 60°$, less than 1% of the trajectories directly penetrate the lowest-density SAMs at both $E_{coll} = 60$ and 80 kJ/mol. Regarding energy transfer, our calculations indicate that trajectories following a direct-penetration mechanism are more efficient in transferring energy to the surface than the rest of the single-

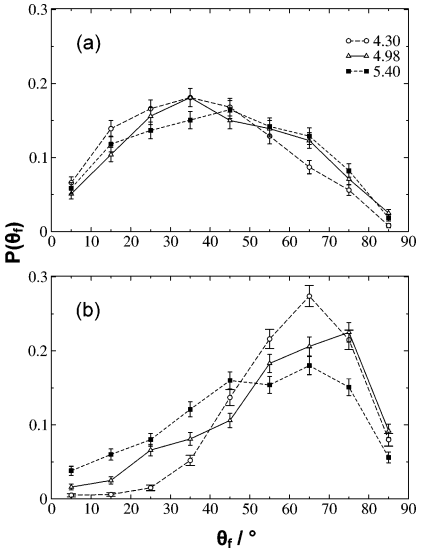

Figure 7. Polar-angle distributions of Ar scattering from dodecanethiolate SAMs at $E_{coll} = 80$ kJ/mol for various lattice spacings of the SAMs. Incident angle: (a) 30 and (b) 60°. The legend indicates the lattice spacings in angstroms.

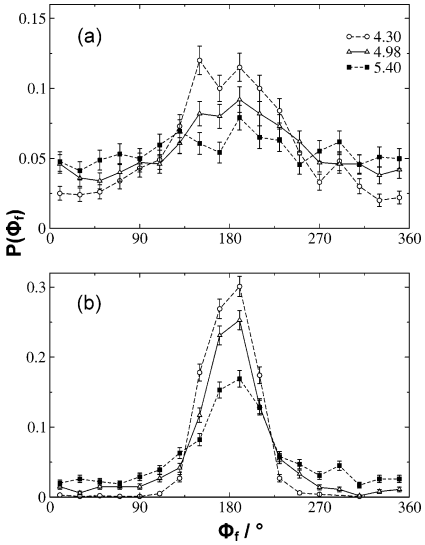

Figure 8. Azimuthal-angle distributions of Ar scattering from dodecanethiolate SAMs at $E_{coll} = 80$ kJ/mol for various lattice spacings of the SAMs. Incident angle: (a) 30 and (b) 60°. The legend indicates the lattice spacings in angstroms.

turning-point collisions (impulsive scattering). For instance, at $E_{coll} = 60$ kJ/mol and with $\theta_i = 30°$, the average energy of the recoiling Ar atoms in direct-penetration trajectories is about 40% smaller than the average energy of impulsively scattered trajectories from the SAM with a 5.4 Å lattice spacing ($\langle E'_T \rangle =$ 6.1 and 10.0 kJ/mol, respectively). Under these same conditions, but $E_{coll} = 80$ kJ/mol, the average product energies of direct-penetration and impulsive-scattering events are 7.1 and 10.1 kJ/mol, respectively. These results indicate that direct penetration of the surface is more probable with less tightly packed SAMs, which in turn leads to a more effective energy transfer.

The number of total trajectories (including both trapping−desorption and direct penetration mechanisms) in which the *z*-coordinate of the Ar atom falls below 1 Å of the average height of the methyl termini of the surface also increases with increasing lattice spacing. There is no surface penetration for SAMs with lattice spacings below that of alkanethiolate SAMs on gold (4.98 Å) at 60 or 80 kJ/mol and $\theta_i = 30$ or 60°. However, Ar atoms readily penetrate SAMs with a lower density, and for a SAM with a lattice spacing of 5.4 Å, ≈23% of the trajectories penetrate the SAM at both 60 and 80 kJ/mol collision energy with $\theta_i = 30°$. The percentage of penetrating trajectories drops to ≈6% with $\theta_i = 60°$ for the two collision energies explored.

(c) Effects on Polar and Azimuthal Angular Distributions. Figure 7 shows the probability distributions of the angle formed by the velocity vector of the recoiling Ar atom with respect to the surface normal (final polar angle, θ_f) for three representative SAMs studied in this work at $E_{coll} = 80$ kJ/mol. For a 30° incident polar angle (Figure 7a), we see that the distributions are largely independent of the SAM interchain separation. The final polar-angle distributions are quite broad, peaking somewhere between 30 and 50°, but exhibiting substantial population in the near-normal ($\theta_f < 10°$) and near-parallel ($\theta_f > 70°$) directions. The probability distributions of Figure 4 indicate that the number of trapping−desorption trajectories increases sharply with increasing lattice spacing, with more than 60% of the trajectories exhibiting trapping−desorption for a 5.4 Å SAM. In addition, for this lattice spacing, ≈23% of the trajectories penetrate the surface. Trapping−desorption is traditionally associated with angular distributions peaking at the surface normal and having a cosine shape.[22,44] However, Figure 7a shows that even when more than 60% of the trajectories bounce several times on the surface, and about a quarter of them penetrate the surface, the scattering distributions do not have cosine shape. This behavior indicates that the traditional patterns of gas/surface scattering do not necessarily apply to noble-gas/organic-surface systems.

The behavior changes when Ar approaches the surface with a 60° incident angle (Figure 7b). The final polar-angle distributions at this incident angle are much more sharply peaked. In addition, there is a clear broadening of the distributions with increasing lattice spacing in the SAMs. All of the distributions peak slightly above 60°. Near-normal scattering is negligible for the tighter SAM, but it is not for more loosely packed SAMs.

Figure 8 shows the final azimuthal angle (Φ_f) probability distributions. The final azimuthal angle is defined as the angle formed between the projections of the initial and final Ar velocity vectors on the plane of the surface, with $\Phi_f = 180°$ indicating in-plane-forward scattering. Much as we have seen in the final polar-angle distributions, the final azimuthal-angle distributions are very broad for a 30° incident polar angle (Figure 8a), and much sharper for a 60° incident polar angle (Figure 8b). The distributions become broader with increasing SAM lattice spacing for both incident angles. The final azimuthal angle distributions are peaked in the in-plane-forward direction ($\Phi_f = 180°$) for the less dense SAMs at a 60° incident angle, but the distributions flatten with increasing SAM lattice spacing at a 30° incident angle.

The angular distributions for an incident angle of 60° (Figures 7b and 8b) can be rationalized as follows. For the more tightly packed SAM, the sharply peaked azimuthal-angle and polar-angle distributions indicate that the scattering dynamics is dominated by specular events. A decrease in the density of the SAMs results in a decrease of the specular component of the angular distributions, which is characterized by a broadening in the azimuthal distributions, and a larger probability for final polar angles well below 60° in the polar-angle distributions. The angular distributions for an incident angle of 30° (Figures 7a and 8a) do not follow this trend completely. Specular scattering is not clearly dominating the total scattering for the more tightly packed SAM. Although the final polar-angle

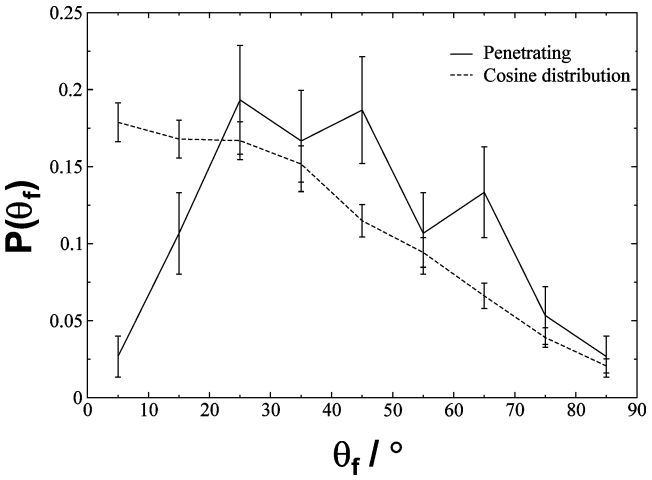

Figure 9. Polar-angle distribution of Ar atoms desorbed from dodecanethiolate SAMs after penetration compared with a distribution calculated considering that all of the trajectories desorb with a polar angle sampled from a cosine function: $E_{coll} = 80$ kJ/mol, $\theta_i = 30°$, and lattice spacing = 5.4 Å.

distributions peak at the incident angle (30°), the azimuthal-angle distributions do not peak sharply at 180°. Furthermore, the azimuthal-angle distributions become nearly uniform for the more loosely packed SAMs. This trend concurs with the increased probability for trapping−desorption events in which the desorbing atom has lost the memory of its initial direction.

Although trapping−desorption dominates the microscopic mechanism of the collisions for the less dense SAMs explored in this study for $\theta_i = 30°$, the expected cosine shape of the polar-angle distributions is not observed. Instead, the distributions are quite broad and peak in the 30−50° interval. To further illustrate this behavior, we show in Figure 9 the final polar-angle distributions of the trajectories that penetrate the SAM with a 5.4 Å lattice spacing at $E_{coll} = 80$ kJ/mol and $\theta_i = 30°$, in comparison with a cosine distribution. The model distribution has been obtained assuming that all of the trajectories considered in the calculations of Figure 9 desorb with a cosine distribution.[22,44] The figure shows that surface penetration does not imply polar angles of desorption distributed according to a cosine function. Trajectory animation indicates that Ar atoms trapped inside the surface tend to scatter along the tilt direction, and thereby the polar-angle distributions peak in the 25−45° angular interval (tilt angle for this SAM = 36°). We note that this behavior has been recently found in experiments of hyperthermal Xe scattering from SAMs on gold by Sibener and co-workers, in which Xe penetration in the SAMs was found to be substantial.[45]

Concluding Remarks

We have studied collisions of superthermal Ar atoms with dodecanethiolate self-assembled monolayers of different densities using the classical trajectory method with a potential energy surface that has been shown to be accurate in earlier studies. The calculations are motivated by recent molecular-beam experiments using alkanethiolate SAMs grown on gold and silver (4.98 and 4.67 Å lattice spacings, respectively).

We find that tightly packed SAMs reduce the amount of energy transfer from the Ar atom to the SAM, in agreement with experiments. Our calculations indicate that there are several reasons for this behavior. First, loosely packed SAMs promote a longer residence time of Ar on the surface, which facilitates energy transfer. Second, in trajectories in which there is a single encounter between the Ar atom and the SAM, energy transfer to the less dense SAMs is more efficient. This behavior seems tied to a decrease in the vibrational frequencies of large-amplitude modes that absorb the excess energy in the less dense SAMs. Finally, Ar atoms can penetrate the organic monolayers with longer lattice spacings, which allows for intimate interaction between the gas-phase species and the alkane chains, subsequently enhancing energy transfer.

Our calculations reveal the expected trend that energy transfer is more efficient for more perpendicular approaches of Ar to the surface. Trapping−desorption and surface penetration are seen to be larger for a 30° incident angle than for a 60° incident angle. Analysis of angular distributions reveals that specular scattering is favored for the more glancing collisions ($\theta_i = 60°$). In contrast, we observe a novel trend in the final polar-angle distributions for an incident angle of 30°. The polar-angle distribution of collisions involving the lowest-density SAM does not have a cosine shape, although 60% of the trajectories undergo a trapping−desorption mechanism and ≈23% of the trajectories penetrate the surface. Instead, there is a preference for desorption along the chain-tilt direction. This behavior indicates that the archetypal cosine desorption traditionally associated with trapping-desorption processes in gas/surface scattering does not necessarily apply to noble-gas/organic-surface scattering in the presence of surface penetration.

Acknowledgment. The work of B.S.D and J.R.M has been supported by the National Science Foundation (CAREER Award No. CHE-94269) and the work of W.A.A. has been supported by NSF Project DMR-0244141: "REU Site: Adhesion Science at Virginia Tech". D.T. is thankful to Virginia Tech for providing a new-faculty start-up fellowship. The authors thank Professor Bill Hase (Texas Tech) and Steven Sibener (University of Chicago) for fruitful discussions.

References and Notes

(1) Miller, D. R. In *Atomic and Molecular Beam Methods*; Scoles, G., Ed.; Oxford University Press: New York, 1988; Vol. 1, p 14.
(2) Weinberg, W. H. In *Dynamics of Gas−Surface Interactions*; Rettner, C. T., Ashfold, M. N. R., Eds.; Royal Society of Chemistry: London, 1991; p 171.
(3) Cardillo, M. J. *Annu. Rev. Phys. Chem.* **1981**, *32*, 331.
(4) Sun, L.; de Sainte Claire, P.; Meroueh, O.; Hase, W. L. *J. Chem. Phys.* **2001**, *114*, 535.
(5) Saecker, M. E.; Govoni, S. T.; Kowalski, D. V.; King, M. E.; Nathanson, G. M. *Science* **1991**, *252*, 1421.
(6) King, K. D.; Fiehrer, M. E.; Nathanson, G. M.; Minton, T. K. *J. Phys. Chem. A* **1997**, *101*, 6556.
(7) King, M. E.; Nathanson, G. M.; Hanning-Lee, M. A.; Minton, T. K. *Phys. Rev. Lett.* **1993**, *70*, 1026.
(8) Nathanson, G. M.; Davidovits, P.; Wornsop, D. R.; Kolb, C. E. *J. Phys. Chem.* **1996**, *100*, 13007.
(9) Lipkin, N.; Gerber, R. B.; Moiseyev, N.; Nathanson, G. M. *J. Chem. Phys.* **1994**, *100*, 8408.
(10) Nathanson, G. M. *Annu. Rev. Phys. Chem.* **2004**, *55*, 231.
(11) Cohen, S. R.; Naaman, R.; Sagiv, J. *Phys. Rev. Lett.* **1987**, *58*, 1208.
(12) Shuler, S. F.; Davis, G. M.; Morris, J. R. *J. Chem. Phys.* **2002**, *116*, 9147.
(13) Day, B. S.; Davis, G. M.; Morris, J. R. *Anal. Chim. Acta* **2003**, *496*, 249.
(14) Day, B. S.; Morris, J. R. *J. Phys. Chem. B* **2003**, *107*, 7120.
(15) Day, B. S.; Shuler, S. F.; Ducre, A.; Morris, J. R. *J. Chem. Phys.* **2003**, *119*, 8084.
(16) Ferguson, M. K.; Lohr, J. R.; Day, B. S.; Morris, J. R. *Phys. Rev. Lett.* **2004**, *92*, 073201.
(17) Isa, N.; Gibson, K. D.; Yan, T.; Hase, W.; Sibener, S. J. *J. Chem. Phys.* **2004**, *120*, 2417.
(18) Gibson, K. D.; Isa, N.; Sibener, S. J. *J. Chem. Phys.* **2003**, *119*, 13083.
(19) Bosio, S. B. M.; Hase, W. L. *J. Chem. Phys.* **1997**, *107*, 9677.
(20) Yan, T.-Y.; Hase, W. L. *Phys. Chem. Chem. Phys.* **2000**, *2*, 901.

(21) Yan, T.-Y.; Hase, W. L. *J. Phys. Chem. B* **2002**, *106*, 8029.
(22) Yan, T.-Y.; Hase, W. L.; Barker, J. R. *Chem. Phys. Lett.* **2000**, *329*, 84.
(23) Yan, T.-Y.; Isa, N.; Gibson, K. D.; Sibener, S. J.; Hase, W. L. *J. Phys. Chem. A* **2003**, *107*, 10600.
(24) Yan, T.-Y.; Hase, W. L. *J. Phys. Chem. A* **2001**, *105*, 2617.
(25) Love, J. C.; Estroff, L. A.; Kriebel, J. K.; Nuzzo, R. G.; Whitesides, G. M. *Chem. Rev.* **2005**, *105*, 1103.
(26) Ullman, A. *Chem. Rev.* **1996**, *96*, 1533.
(27) Ferguson, M. K.; Low, E. R.; Morris, J. R. *Langmuir* **2004**, *20*, 3319.
(28) Schreiber, F. *Prog. Surf. Sci.* **2000**, *65*, 151.
(29) Widrig, C. A.; Alves, C. A.; Porter, M. D. *J. Am. Chem. Soc.* **1991**, *113*, 2805.
(30) Dhirani, A.; Hines, M. A.; Fisher, A. J.; Ismail, O.; Guyot-Sionnest, P. *Langmuir* **1995**, *11*, 2609.
(31) Camilone, N., III; Chidsey, C. E. D.; Eisenberger, P.; Fenter, P.; Li, J.; Liang, K. S.; Liu, G.-Y.; Scoles, G. *J. Chem. Phys.* **1993**, *99*, 744.
(32) Walczak, M. M.; Chung, C.; Stole, S. M.; Widrig, C. A.; Porter, M. D. *J. Am. Chem. Soc.* **1991**, *113*, 2370.
(33) Day, B. S.; Morris, J. R. *J. Chem. Phys.* **2005**, *122*, 234714.
(34) Day, B. S.; Morris, J. R.; Troya, D. *J. Chem. Phys.* **2005**, *122*, 214712.
(35) Jorgensen, W. L.; Maxwell, D. S.; Tirado-Rives, J. *J. Am. Chem. Soc.* **1996**, *118*, 11225.
(36) Jorgensen, W. L.; Tirado-Rives, J. *J. Am. Chem. Soc.* **1988**, *110*, 1657.
(37) Jorgensen, W. L.; Madura, J. D.; Swenson, C. J. *J. Am. Chem. Soc.* **1984**, *106*, 6638.
(38) Liuti, G.; Pirani, F.; Buck, U.; Schmidt, B. *Chem. Phys.* **1988**, *126*, 1.
(39) Ponder, J. W.; Richards, F. M. *J. Comput. Chem.* **1987**, *8*, 1016.
(40) Rappe, A. K.; Casewit, C. J.; Colwell, K. S.; Goddard, W. A., III; Skiff, W. M. *J. Am. Chem. Soc.* **1992**, *114*, 10024.
(41) Frisch, M. J.; Trucks, G. W.; Schlegel, H. B.; Scuseria, G. E.; Robb, M. A.; Cheeseman, J. R.; Montgomery, J., J. A.; Vreven, T.; Kudin, K. N.; Burant, J. C.; Millam, J. M.; Iyengar, S. S.; Tomasi, J.; Barone, V.; Mennucci, B.; Cossi, M.; Scalmani, G.; Rega, N.; Petersson, G. A.; Nakatsuji, H.; Hada, M.; Ehara, M.; Toyota, K.; Fukuda, R.; Hasegawa, J.; Ishida, M.; Nakajima, T.; Honda, Y.; Kitao, O.; Nakai, H.; Klene, M.; Li, X.; Knox, J. E.; Hratchian, H. P.; Cross, J. B.; Bakken, V.; Adamo, C.; Jaramillo, J.; Gomperts, R.; Stratmann, R. E.; Yazyev, O.; Austin, A. J.; Cammi, R.; Pomelli, C.; Ochterski, J. W.; Ayala, P. Y.; Morokuma, K.; Voth, G. A.; Salvador, P.; Dannenberg, J. J.; Zakrzewski, V. G.; Dapprich, S.; Daniels, A. D.; Strain, M. C.; Farkas, O.; Malick, D. K.; Rabuck, A. D.; Raghavachari, K.; Foresman, J. B.; Ortiz, J. V.; Cui, Q.; Baboul, A. G.; Clifford, S.; Cioslowski, J.; Stefanov, B. B.; Liu, G.; Liashenko, A.; Piskorz, P.; Komaromi, I.; Martin, R. L.; Fox, D. J.; Keith, T.; Al-Laham, M. A.; Peng, C. Y.; Nanayakkara, A.; Challacombe, M.; Gill, P. M. W.; Johnson, B.; Chen, W.; Wong, M. W.; Gonzalez, C.; Pople, J. A. *Gaussian 03*, Revision C.02; Gaussian Inc.: Wallingford, CT, 2004.
(42) Lenzer, T.; Luther, K.; Troe, J.; Gilbert, R. G.; Lim, K. F. *J. Chem. Phys.* **1995**, *103*, 626.
(43) Troya, D. *J. Phys. Chem. A* **2005**, *109*, 5814.
(44) Goodman, F. O.; Wachman, H. Y. *Dynamics of Gas−Surface Scattering*; Academic Press: New York, 1976.
(45) Sibener, S. J.; Gibson, K. D.; Isa, N. *J. Phys. Chem.*, submitted for publication.